Dynamic Instabilities of Fracture under Biaxial Strain Using a Phase Field Model

Hervé Henry and Herbert Levine
Center for Theoretical Biological Physics, University of California–San Diego, 9500 Gilman Drive, La Jolla, California 92093, USA
(Received 19 February 2004; published 2 September 2004)

We present a phase-field model of the propagation of fracture under plane strain. This model, based on simple physical considerations, is able to accurately reproduce the different behavior of cracks (the principle of local symmetry, the Griffith and Irwin criteria, and mode-I branching). In addition, we test our model against recent experimental findings showing the presence of oscillating cracks under biaxial load. Our model again reproduces well observed supercritical Hopf bifurcation and is therefore the first simulation which does so.

DOI: 10.1103/PhysRevLett.93.105504 PACS numbers: 62.20.Mk, 02.70.–c, 47.54.+r

In recent years, the physics community has seen a rebirth of interest in the problem of dynamic fracture. This rebirth was kindled by a series of experiments revealing that the current engineering approach to crack propagation, namely, the coupling of linear elasticity to an empirical energy balance law for crack tip motion, cannot account for the richness of actual fracture phenomenology [1]. Specifically, dynamical instabilities which drive the system away from a single crack propagating in a straight line require more sophisticated attention to the actual tip region, the so-called process zone.

Given the above, it is clear that one needs a framework which can couple local degrees of freedom involved in breaking interatomic bonds to global elasticity. *Strain softening* has been used to describe microcracking in the process zone, but this approach allows only the propagation of the crack along the discretization lattice [2,3]. Other approaches using a nonlinear elasticity where the stress fully relaxes at high strain have also been proposed. They require the use of higher order terms to avoid being ill posed and they have not been able to reproduce features of brittle fracture [4]. To circumvent these problems the phase-field modeling of fracture uses an order-parameter field (the degree of ''brokenness'') which then couples to the elastic strain in a manifestly continuum-level formulation. The fact that the system does not need to be placed on a lattice avoids dynamical artifacts associated with the breaking of translational and rotational symmetry of discrete models [5,6]. One such phase-field model [Karma-Kessler-Levine (KKL)] [7] has been shown to correctly encompass much of the expected behavior of mode-III (out-of-plane) cracks [8].

Here, we extend the KKL model to full vector elasticity and test its genericity. Our major interest is in seeing whether a recently discovered supercritical Hopf bifurcation to oscillating cracks under biaxial loading [9] (see Fig. 1) is in fact reproduced by KKL; we see that in fact it is. This successful simulation of the crack oscillation has the dual benefit of demonstrating that the instability is not dependent on any special properties of the specific materials used in the experiment (rubber) and also of giving us more confidence in the phase-field methodology.

We start with the KKL phase-field model [7]. Here, a sheet of fractured elastic material is represented by the elastic displacement field u_x, u_y and by a phase-field variable ϕ that can be interpreted as the proportion of intact interatomic links. The evolution equation of u_x and u_y derives from a modified elastic energy:

$$E = \iint dxdyg(\phi)\left(\frac{1}{2}\lambda\epsilon_{ii}^2 + \mu\epsilon_{ij}^2\right), \tag{1}$$

where $g = (4 - 3\phi)\phi^3$ is a function of ϕ chosen such that $g(0) = 0$, $g(1) = 1$, and $g'(0) = g'(1) = 0$; this specific choice is discussed in [7]. The tensor $\epsilon_{ij} = (\partial_i u_j + \partial_j u_i)/2$ is the strain tensor. The evolution equations for u_x and u_y are then

$$\rho\partial_{tt}u_i = -\frac{\delta E}{\delta u_i}. \tag{2}$$

The corresponding evolution equation of ϕ is

$$\tau\partial_t\phi = \Delta\phi - \frac{dV(\phi)}{d\phi} - \frac{dg(\phi)}{d\phi}(E_\phi - \epsilon_c), \tag{3}$$

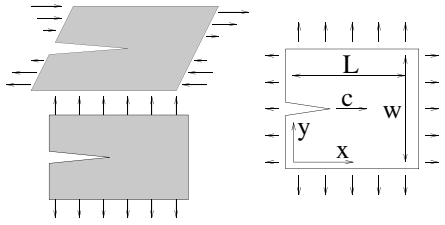

FIG. 1. Left: definition of in-plane loading modes: top—mode-II loading; bottom—mode-I loading. Right: geometry of the experiment reported in [9]. An elastic sheet is extended in both x and y directions. The local strain is bigger in the y direction than in the x direction. The crack speed is denoted by c. In simulations performed here W was taken equal to 60 and at $y = 0$ and $y = W$, u_x was kept constant in time, so that a vertically propagating crack cannot reach $y = W$ or $y = 0$.

where $V(\phi) = 4[\phi(1-\phi)]^2$ is a double well potential and

$$\begin{cases} E_\phi = \frac{1}{2}\lambda\epsilon_{ii}^2 + \mu\epsilon_{ij}^2 & \text{if } \mathrm{tr}(\epsilon) > 0 \\ E_\phi = \frac{1}{2}\lambda\epsilon_{ii}^2 + \mu\epsilon_{ij}^2 - \alpha K_{\mathrm{lame}}\epsilon_{ii}^2 & \text{if } \mathrm{tr}(\epsilon) < 0, \end{cases} \quad (4)$$

where $K_{\mathrm{lame}} = (\lambda + \mu)/2$ is the modulus of compression for a plane strain configuration; α is an arbitrary coefficient chosen to be bigger than 1. This breaking of the symmetry between compression and extension is a key ingredient not present in previous phase-field approaches to in-plane fracture [10,11]. In our model, if a material is simply compressed, having $\alpha > 1$ will guarantee that it will not break; also, compression will increase the threshold needed for inducing a fracture through shear. The parameters values used here are $\epsilon_c = 1$, $\tau = 5$, $\lambda = \mu = 1$, and $\alpha = 1.5$.

We proceed to study this model computationally in a box of width W and length L. Simulations were performed using a grid spacing of $\delta x = 0.15$ and a time step of $\delta t = 0.001$. (Decreasing to $\delta x = 0.075$ and $\delta t = 0.0005$ leads to no significant difference in the results.) The time stepping scheme was the forward Euler method while the spatial operators were computed using a discretization that conserves the discretized energy of Eq. (1). (The use of other scheme leads to long term numerical instabilities.) In our simulations, we used both fixed grids of different sizes along the x axis and a grid moving with the fracture tip along the x axis. Boundary conditions for the fixed grid were as follows: at the $y = W$ ($y = 0$) boundary, u_y was kept equal to Δ_y (0) and on both lateral edges $u_x = x\Delta_x/L$. At the $x = L$ ($x = 0$) boundary, u_x was kept equal to Δ_x (0) and no flux boundaries were used for the u_y field. In the case of the moving grid, the boundary conditions at $y = W$ and $y = 0$ were unchanged whereas the boundary conditions at the horizontal ends of the grid were modified. First we introduced an artificial viscosity in a thin layer at both ends. (This mimics partially absorbing boundary conditions.) Also, at the leftmost end the u_x field was kept constant between each displacement of the grid. We checked that those modifications did not affect the behavior of the crack when compared to results obtained using a long enough fixed grid, thereby allowing us to simulate the crack propagation along an infinite strip along the x axis. The initial conditions were constructed as follows: a small initial crack was created by setting $\phi = 0$ in a small region of fixed width and variable length and by letting the system evolve following a damped version (see later) of the evolution equation of elasticity (while ϕ was kept constant) until a stationary state was reached.

We first tested the model for damped dynamics obtained by replacing ∂_{tt} by ∂_t. For pure mode-I loading, the fracture began to propagate once the imposed elastic energy was higher than the fracture energy (see later). In addition, in this case, the stress intensity factor at the tip of a steady crack was found to be constant for various loading configuration, hence obeying the Irwin criterion [12] (data not shown). More interestingly, numerical simulations in the case of pure mode-II loading showed that the model respects the local symmetry principle: the fracture propagates in the direction which nullifies the stress intensity factor for mode II [see Fig. 2 (right)]. Hence this model reproduces well the behavior of a single crack in the damped regime. Note that this result depends on our asymmetry parameter α; allowing breakage under compression leads to a model which does not follow the local symmetry principle [Fig. 2 (inset in the right panel)]. The results for different α ranging from 1 to 2 were similar.

Next, we turn briefly to results obtained in the dynamic (nondamped) case under pure mode-I loading. As expected by analogy with the results of [7] for the case of mode-III loading, the initiation of crack propagation appeared at the Griffith threshold with good accuracy. Indeed, according to the Griffith criterion, one would expect a crack to begin to propagate for a value of the y extension Δ_y bigger than Δ_c which is a solution of

$$W\left[\left(\frac{1}{2}\lambda + \mu\right)\frac{\Delta_c^2}{W^2}\right] = 2\int_0^1 d\phi\sqrt{2[1 - g(\phi)] + V(\phi)}. \quad (5)$$

This formula was derived in [7] and follows from the asymptotic solution of the model in the region far behind the crack tip. For the parameter values used here, this threshold is at 9.5 whereas in our simulations the crack

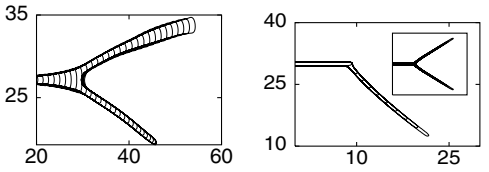

FIG. 2. Left: contour plot of the line $\phi = 0.5$ taken at 1 time unit (t.u.) intervals during the branching of a crack under mode-I loading with $\Delta_y = 18$ and $\beta = 1$. The angle of the two branches at the branching site is approximately 40°, and the critical speed for which the instability occurs is approximately 0.5 while the shear speed is 1, which is in agreement with predictions in [13]. During the evolution of the system, the lower branch will recede while the upper branch will propagate and branch irregularly. The simulations are performed using the undamped model. Right: contour plots of $\phi = 0.5$ taken at 40 t.u. during the propagation of an overdamped crack in a medium where pure mode-II loading is applied. The initial crack is straight and oriented along the x axis. The crack propagates in a direction that nullifies the mode-II stress intensity factor. Inset: same parameters with $\alpha = 0$. One can see that, in this case, the crack branches and propagates in two directions symmetrical with respect to the x axis. The second branch propagates in a region where the material is strongly compressed.

begins to propagate for Δ_y bigger than 9.7 ± 0.1; this 2% discrepancy is due to discretization and finite width effects and gives some measure of the accuracy of our computations. The speed of the stable crack behaved qualitatively as expected when loading was increased. When loading was further increased, the dynamic fracture exhibits a branching instability and a secondary crack begins to propagate (see Fig. 2). This branching instability is compatible with what has been observed experimentally in a wide range of materials [14,15].

We now turn to our major interest here, the case of a dynamic crack propagating under biaxial stress. Experimental work by Deegan *et al.* [9] has shown that for a given imposed strain in the y direction (see Fig. 1), there is a threshold value of the x strain for which the crack propagation is no longer straight; instead, the crack tip position begins to oscillate. In fact, the instability appears to be supercritical and the tip trajectory is well approximated by a sinusoidal line with finite wavelength and amplitude. Recall that in our calculations strains are applied by moving the rightmost border of the sheet by Δ_x and by moving the top border by Δ_y; hence, if $\Delta_x = 0$, the system is set to pure mode I. The experimental results translate into the prediction of a Hopf bifurcation that should occur as we cross a threshold value of $r = W\Delta_x/L$, with Δ_y being fixed.

The results of our numerical simulations for two sets of λ, μ and different values of Δ_y faithfully reproduce the aforementioned phenomenology. Namely, the fracture tip trajectory indeed undergoes a Hopf bifurcation when the x extension is increased over a threshold value that depends on both parameter regime and the vertical extension. This bifurcation is characterized by the fact that below threshold, the tip position shows damped oscillations (see Fig. 3) and ends up propagating along a straight line, whereas above threshold those oscillations are amplified and the restabilized state corresponds to the situation where the fracture tip oscillates at a finite wavelength with a finite amplitude (see Fig. 3). We checked that this instability was not due to waves reflecting at the boundaries that can create periodic markings called Wallner lines [16]. Indeed, the expected wavelength of such markings would be $\lambda = Wv/c\sqrt{1 - v^2/c^2}$, that is about 10 s.u. while the wavelength observed here is about 300 s.u. This is confirmed by the fact that switching to quasiabsorbing boundary conditions at the $y = W$ and $y = 0$ lines does not affect the oscillations.

When the restabilized state is reached, the trajectory of the tip is almost indistinguishable from a sinusoidal line, as in [9]. One can also note that the horizontal tip speed oscillates with a frequency equal to 2 times the frequency of the vertical position, so that the maximum of the horizontal tip speed is reached when the instantaneous tip velocity is directed along the x axis. In addition, the tip speed tangent to its trajectory is kept almost constant

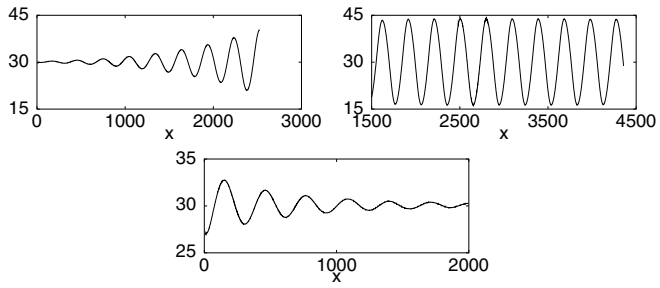

FIG. 3. Fracture tip trajectories for $\Delta_y = 10$ and $r = W\Delta_x/L = 8.0$ during the transient regime (a) and when a stationary state is reached (b). The steady-state tip trajectory matches a simple sinusoid. (c) Tip trajectory for $\Delta_y = 10$ and $r = W\Delta_x/L = 7.25$, exhibiting damped oscillations. In (b) the mean tip speed is 0.362 and the mean tip speed along the x axis is 0.354. In (c), the tip speed is 0.347 once straight propagation has resumed. The transverse and longitudinal speeds of sound are, respectively, 1 and 1.22. The period of the oscillations in (b) is about 831 t.u. and the corresponding wavelength is 294 s.u.

(up to numerical errors) and for different values of r (r varying between 7 and 8), we did not find significant changes in the tip speed (less than a few %). A picture of this state is presented in Fig. 4.

We now describe the changes in the oscillating restabilized state when the strain along the x axis is increased. As seen in Fig. 5, the amplitude of the oscillations behaves like $\sqrt{\Delta_x - \Delta_{xc}}$ close to threshold, which is consistent with a supercritical Hopf bifurcation, as experimentally observed in [9]. The wavelength and period of the tip oscillation decreases slightly when $\Delta_x - \Delta_{xc}$ is increased; this differs from results in [9] where the wavelength increases when $\Delta_x - \Delta_{xc}$. This may be due to nonlinear elasticity effects present in the experiment.

We also performed numerical simulations with biaxial strain and $\alpha = 0$. The results obtained did not differ significantly from that observed for $\alpha = 1.5$. This is somewhat surprising, since the simplest interpretation of the oscillations observed here suggests that the mechanism is at least partially similar to the one underlying

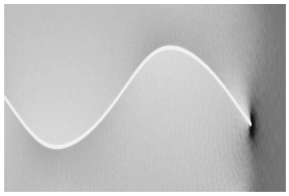

FIG. 4. Elastic energy landscape (gray scale, dark regions correspond to high density) during the propagation of an oscillating crack. The white region corresponds to the broken region ($\phi < 0.5$). Parameter values are as in Fig. 3(a). Between the arches of the sinusoidal line of the crack, the elastic energy density is lower than in the vicinity of the upper and lower boundaries of the slice.

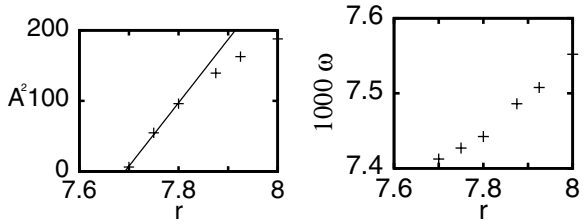

FIG. 5. (a) Square of the amplitude of the oscillations as a function of $r = W\Delta_x/L$. (b) Frequency ω (+) of the oscillations. The wavelength (not shown) varies like the inverse of ω since the crack speed is not varying much (about 10^{-3}) over the parameter range presented here.

oscillations of a quasistatic crack propagating in a thermal gradient [17,18]. In that case, theoretical work has explained the transition to an oscillating crack using a (modified) principle of local symmetry [19,20]; changing the tip direction induces a mode-II component which causes further deviation from the original line. We have already shown that this principle does not apply for a symmetric model for pure mode-II loading. Perhaps the explicit breaking of the symmetry by the mode-I part of the driving is enough to suppress the unphysical compressional breaking for the case of $\alpha = 0$, and hence this model still exhibits the Hopf bifurcation. In support of this, we verified that even in this case, a crack tip with damped dynamics will obey the principle of local symmetry, if in addition to a pure mode-II load one adds a small mode-I extension. We should note, though, that we never observe oscillations with damped dynamics, even when r was set to very close to Δ_y, i.e., close to hydrostatic strain. However, increasing τ (up to 50), i.e., increasing the dissipation at the crack tip, did not affect significantly either the instability wavelength of the oscillating crack or the threshold but did reduce the crack speed [from 0.362 to 0.05 ($\tau = 50$)]. Also, changes in Δ_y ($\Delta_y = 12, 14$, with $\tau = 20$ to avoid branching) did not affect significantly the wavelength of the oscillating crack but did change the threshold. Interestingly, the wavelength scales linearly with W. Hence, it seems that the saturation of the amplitude is governed by the interaction of the tip with the sidewall. Underlying the actual instability is perhaps the simple fact that an oscillating crack will alleviate extra elastic energy under biaxial strain.

In summary, this Letter shows that the extension of the KKL phase-field model of crack propagation to full vector elasticity qualitatively reproduces the different instabilities observed when considering the propagation of cracks. One should note that with an extremely simple model based on generic physical considerations we were nonetheless able to reproduce the variety of observed patterns. This lends confidence in the entire modeling approach and suggests that we proceed in two complementary directions. First, we can continue to investigate the phenomenology of KKL, specifically looking at the interaction of different cracks (the phase-field method can easily deal with intersecting interfaces) and also truly three-dimensional effects [21]. At the same time, it is time to begin understanding how to combine this method with microscopic interaction data about specific materials so as to enable the building of more quantitatively reliable models of dynamic fracture.

It is a pleasure to acknowledge useful discussions with A. Karma and D. Kessler. This research is supported by the National Science Foundation through Grant No. DMR-0101793.

[1] J. Fineberg and M. Marder, Phys. Rep. **313**, 1 (1999).
[2] X. Xu and A. Needleman, J. Mech. Phys. Solids **42**, 1397 (1994).
[3] M. Falk, A. Needleman, and J. Rice, J. Phys. IV (France) **11**, 43 (2001).
[4] R. H. J. Peerlings, R. de Borst, W. A. M. Brekelmans, J. H. P. de Vree, and I. Spee, Eur. J. Mech. A **15**, 937 (1996).
[5] D. Kessler and H. Levine, Phys. Rev. E **68**, 036118 (2003).
[6] S. P. Gross and M. Marder, J. Mech. Phys. Solids **43**, 1 (1995).
[7] A. Karma, D. Kessler, and H. Levine, Phys. Rev. Lett. **87**, 045501 (2001).
[8] A. Karma and A. Lobkovski, Phys. Rev. Lett. **92**, 245510 (2004).
[9] R. Deegan, P. Petersan, M. Marder, and H. Swinney, Phys. Rev. Lett. **88**, 014304 (2002).
[10] I. S. Aranson, V. A. Kalatsky, and V. M. Vonokur, Phys. Rev. Lett. **85**, 118 (2000).
[11] L. Eastgate, J. Sethna, M. Rauscher, T. Cretegny, C.-S. Chen, and C. Myers, Phys. Rev. E **65**, 36117 (2002).
[12] L. Freund, *Dynamic Fracture Mechanics* (Cambridge University Press, Cambridge, U.K., 1990).
[13] M. Adda-Bedia, J. Mech. Phys. Solids (to be published).
[14] J. Fineberg, S. P. Gross, M. Marder, and H. L. Swinney, Phys. Rev. Lett. **67**, 457 (1991).
[15] K. Ravi-Chandar and W. G. Knauss, Int. J. Fract. **25**, 247 (1984).
[16] B. Lawn, *Fracture of Brittle Solid* (Cambridge University Press, Cambridge, U.K., 1993), 2nd ed.
[17] M. Adda-Bedia and Y. Pomeau, Phys. Rev. E **52**, 4105 (1995).
[18] A. Yuse and M. Sano, Nature (London) **362**, 329 (1993).
[19] J. Hodgdon and J. Sethna, Phys. Rev. B **47**, 4831 (1993).
[20] E. Bouchbinder, H. Hentschel, and I. Procaccia, Phys. Rev. E **68**, 036601 (2003).
[21] E. Sharon, G. Cohen, and J. Fineberg, Nature (London) **410**, 68 (2001).